Adsorption of Pd, Pt, Cu, Ag and Au Monomers on NiAl(110) Surface: a Comparative Study from DFT Calculations.

ARTICLE *in* THE JOURNAL OF PHYSICAL CHEMISTRY A · NOVEMBER 2013

Impact Factor: 2.69 · DOI: 10.1021/jp405877k · Source: PubMed

3 AUTHORS:

Miguel San-Miguel
University of Campinas
53 PUBLICATIONS **749** CITATIONS
SEE PROFILE

Edgard Pacheco Moreira Amorim
Universidade do Estado de Santa Catarina
12 PUBLICATIONS **79** CITATIONS
SEE PROFILE

Edison Z. da Silva
University of Campinas
70 PUBLICATIONS **868** CITATIONS
SEE PROFILE

THE JOURNAL OF PHYSICAL CHEMISTRY A

Article

pubs.acs.org/JPCA

Adsorption of Pd, Pt, Cu, Ag, and Au Monomers on NiAl(110) Surface: A Comparative Study from DFT Calculations

Miguel A. San-Miguel,[†] Edgard P. M. Amorim,[‡] and E. Z. da Silva*[,§]

[†]Physical Chemistry Department, University of Seville, E41012 Seville, Spain

[‡]Departamento de Física, Universidade do Estado de Santa Catarina, 89219-710 Joinville, SC, Brazil

[§]Institute of Physics "Gleb Wataghin", University of Campinas, Unicamp, 13083-970 Campinas, SP, Brazil

ABSTRACT: First principles calculations based on periodic density functional theory (DFT) have been used to investigate the structural, energetic and electronic properties of different transition metal atoms (Pd, Pt, Cu, Ag, and Au) on the NiAl(110) surface at low coverages (0.08 and 0.25 monolayer). All adatoms prefer to adsorb on 4-fold coordinated sites interacting with two Al and two Ni atoms and forming polar and covalent bonds, respectively. The calculated negative work function changes are explained by the effect of positive surface image created after adsorption, which induces the polarization of the negatively charged adsorbates. Consequently, for metals with similar electronegativity as Ni (Ag and Cu), this polarization effect becomes more significant and leads to larger negative work function changes, but the charge transferred is small.

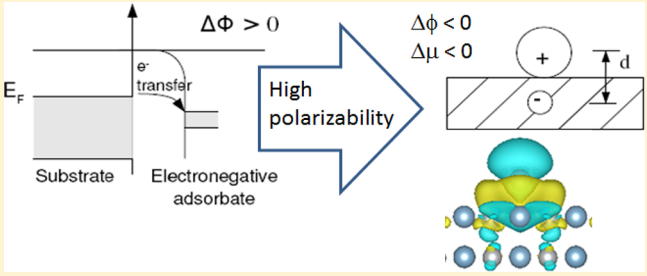

INTRODUCTION

Among the bimetallic alloys, NiAl has gained a wide popularity because of some industrial applications. In particular, since they are lightweight materials, resistant to corrosion, and have high temperature melting points, they are extensively used in aerospace industry.[1] NiAl oxidizes easily forming a thin coherent Al_2O_3 film. The stability of these films has major importance when using as thermal barrier coatings (TBCs) in materials exposed to harsh conditions such as jet turbine engines. The oxidation process and the structure of the formed oxide have been addressed in the literature.[2−6] Commonly, some late transition metals (Pd, Pt, and Ir) are also added to the NiAl surface because they seem to improve the adhesion of the Al_2O_3 films to the metal substrate extending the lifetime of the TBC.[7,8] However, the origin of this effect is not well understood yet. Similarly, other species such as La, Hf, Y, and Zr are added because they provoke the reactive element effect (REE) so improving the resistance to higher temperatures.[9,10] During the manufacturing process, other impurities such as sulfur can also be present, and they can play a different role promoting negative effects on the adhesion of the Al_2O_3 films.

The β-NiAl is a stable phase that also has been used broadly in Surface Science. It crystallizes in the CsCl B2 structure (bcc). The lowest energy surface corresponds to the NiAl(110) surface. This is a close packed and stoichiometric surface. It exhibits equal amounts of Ni and Al atoms that are organized in alternating rows. The NiAl(110) surface has been studied using both experimental and theoretical methods.[11−21] Since the earlier studies using low energy electron diffraction (LEED)[11] and medium energy ion scattering (MEIS)[12] techniques, it is well-known that this surface relaxes to a rippled structure in which the top Al rows rise up, while the Ni rows move downward reducing efficiently the surface strain.[13,14,18,19] The NiAl(110) surface has been used as catalytic substrate for H_2 decomposition,[22] and there are also some experimental evidences of methanol and water decomposition but still scarce theoretical studies.[23−26] Some experimentalists have used NiAl(110) surfaces to grow epitaxial Al_2O_3 films with controlled thickness for studying catalytic properties of supported metal clusters.[27−31] A recent study has investigated the conditions at which OH and CO can adsorb on NiAl(110) and play a role as precursors for nucleating graphite or aluminum oxide on the surface.[21]

The NiAl(110) surface is also a favorite substrate used to study supported nanostructures, particularly since Nilius et al. showed a way to assemble Au atoms to form linear atomic chains (LACs) on the NiAl(110) surface, using scanning tunneling microscopy (STM) techniques.[32] To gain insight into the experimental observations on these nanostructures,[33−37] different authors have employed theoretical methods to address the adsorption of different metal atoms or LACs on the NiAl(110) surface.[18,32,34,38−44] Other studies have focused on other more complex structures of Ag and Au, including monolayer and multilayer formations, and also codeposition of Ni and Al on the NiAl(110) surface.[45−50]

Special Issue: Energetics and Dynamics of Molecules, Solids, and Surfaces - QUITEL 2012

Received: June 14, 2013
Revised: October 31, 2013
Published: November 12, 2013

However, there are still some open questions regarding the nature of the bonding between single impurities and the substrate. In this work, we have performed a systematic investigation of late transition metal monomers adsorbed on the NiAl(110) surface. We have analyzed the preferable adsorption sites for each monomer, and we provide new insights into the nature of the chemical bonding from calculated dipole moment and work function changes and charge distributions. Although, other authors have addressed the adsorption sites for some of the monomers,[18,34,38,39] they have not dealt with the changes of the work function upon adsorption. The study of the work function aids to the understanding of the bonding formed by the single impurities and the surface atoms and show new interesting trends because the calculated work function changes do not follow the accepted general behavior.

The work function Φ is a key electronic property in surface science. It is defined as the minimum energy required to remove an electron from the highest occupied energy level in the substrate (Fermi level) to the vacuum level, and it can be estimated by photoelectron spectroscopy (PES) techniques. Variations of work function $\Delta\Phi$ upon adsorption provide significant insights on the charge transfer process. Traditionally, electronegative adsorbates are related to work function increases because the adsorbate withdraws electron density from the surface creating a dipole in the same direction as for the clean surface. Differently, electropositive adsorbates donate electron density to the surface and consequently the dipole produced is in the opposite direction to that of the clean surface, and the work function decreases. Although this general model has been used successfully for a large number of adsorption systems, there have been reported different systems in which the electron transfer from the surface to the adsorbate induces an unexpected work function decrease. Thus, N on W(100) is a well-known case. N chemisorption on most well-defined W crystal faces leads to work function increase; however, the adsorption on W(100) and some other faces decreases the work function.[51−53] According to the general interpretation this would mean that N takes positive or negative charge depending on the crystal face. Michaelides et al. demonstrated that the work function decrease induced by N adsorption on W(100) is consistent with a negative charge on N, and the reason for this unexpected behavior is the overspill electron density into the vacuum.[54] A similar discussion was previously reported by Pettersson and Bagus[55] when they studied Cl on Cu(100) by using a Hartree−Fock cluster model approach. They showed that a small reduction in the surface dipole moment is compatible with a large negative charge on the adsorbate. Hence, they concluded that work function changes do not necessarily account for the adsorbate ionicity.

Other authors have found systems in which similar irregularities can be observed. Thus, the adsorption of I to Ni(100)[56] or Pt (111)[57] has been reported as inducing charge transfer from the surface to the adsorbate and decreasing the work function by around 1 eV. Migani et al. reported that the work function change induced by the presence of an adsorbed halide can be either positive or negative, depending on the surface metal.[58] Leung et al. investigated a large number of elements adsorbed on various orientations of W substrates and demonstrated that the standard electronegativity scale can predict reliably the direction of charge transfer but not necessarily the adsorbate induced change in the work function.[59] In the present study, we analyze the structural and electronic properties of the adsorption on the NiAl(110) surface of different transition metal monomers from groups 10 (Pd and Pt) and 11 (Cu, Ag, and Au). Thus, we intend to rationalize the nature of the bonding between each monomer and the NiAl(110) surface. To achieve this, we analyze the different adsorption sites to find the most favorable ones, we look at the distribution of charge density, and we discuss why the work function changes upon adsorption do not follow the general expected behavior.

METHODS

Calculations were performed within the density functional theory (DFT) using the plane wave pseudopotential VASP code.[60−62] The projector augmented wave (PAW) method was applied to describe electron−ion interactions.[63−65] The generalized gradient approximation (GGA) in the Perdue−Wang parametrization is used for the electron exchange and correlation contribution to the total energy.[66,67] A kinetic energy cutoff of 300 eV is used for all systems, which is adequate to obtain total energies converged to at least 1 meV/atom. The Brillouin zone was integrated using the Methfessel−Paxton smearing method, with a smearing width of 0.1 eV. Conjugated gradient (CG) energy minimization method is used to obtain relaxed bulk, surface, and adsorption systems. Atoms are fully relaxed until the Hellmann−Feynman forces converged to less than 0.01 eV/Å per atom. Since NiAl is a nonmagnetic alloy with a filled d band there is no need to perform spin-polarized calculations. We checked out this aspect and results showed that the energy difference between spin-polarized and nonspin-polarized is about 1 meV/atom. For the adsorption systems, we also carried out spin-polarized calculations for the most representative cases discussed in the results section, and no appreciable differences were observed.

Bulk NiAl is a body centered cubic (bcc) structure with two atoms in the primitive unit cell. The use of a 11 × 11 × 11 Monkhorst−Pack k-point grid yields lattice parameter, bulk modulus, and cohesion energy with deviations from the experimental values[68] of 1%, 3%, and 8%, respectively, which is a good agreement at low computational cost.

The low index NiAl(110) surface was modeled using three different supercells. In the first one, the primitive unit cell with two atoms was replicated to form a 25 layers slab (1 × 1 × 25 model). The other two are five layer-thick slabs with 2 × 2 and 3 × 4 unit cells (2 × 2 × 5 and 3 × 4 × 5 models). Additional calculations were carried out for the most representative scenarios using 3 × 4 × 7 slabs, and no differences with respect to the 3 × 4 × 5 were observed.

In all models the atomic positions for the two bottom layers are fixed to the original bulk positions. The surface unit cell has lengths of $a_0\sqrt{2}$ and a_0 along the $[\bar{1}10]$ and $[001]$ directions where a_0 is the calculated lattice parameter (2.91 Å). The vacuum distance in the surface normal direction is set to 12 Å, which is large enough to avoid the interaction between the surface and its images and also to guarantee meaningful calculations of the work function.

In order to test these models, we have computed the surface energy (γ) and some structural parameters such as the rippling distance between Ni and Al atoms from the top layer (Δ_{11}), the interlayer distances between the first and second layer and between the second and third layer for each element compared to the experimental bulk distance (d_{12} and d_{23}, respectively). Two different Monkhorst−Pack k-point grids (15 × 21 × 1 and 7 × 9 × 1 grids) have been compared for the 1 × 1 × 25 and 2

dx.doi.org/10.1021/jp405877k | J. Phys. Chem. A 2014, 118, 5748−5755

Table 1. NiAl(110) Supercells in Unit Cell Units, Monkhorst–Pack Grids, Surface Energy (γ), Rippling (Δ_{11}), and Interlayer Distances (d_{12} and d_{23}) in Percent of the Experimental Bulk Distance (2.046 Å) between Ni and Al Atoms in the Three Top Layers

	surfaces (u.c.)	k-points	γ (J/m^2)	Δ_{11} (Å)	d_{12} (%) Ni/Al	d_{23} (%) Ni/Al
this work	1 × 1 × 25	15 × 21 × 1	1.516	0.14	−2.04/+2.55	−2.15/+1.43
	2 × 2 × 5	7 × 9 × 1	1.574	0.16	−3.49/+2.13	−1.13/+1.98
	3 × 4 × 5	5 × 5 × 1	1.568	0.16	−3.03/+2.12	−1.89/+1.01
ref 18 (DFT)	2 × 2 × 5	7 × 9 × 1	1.569	0.17	−3.0/+3.0	−1.65/+1.0
ref 11 (LEED)				0.22	−6.0 ± 1/+4.6 ± 1	
ref 12 (MEIS)				0.204	−7 ± 1/+5 ± 1	+1 ± 2/−1 ± 2

× 2 × 5 supercells, and only the 7 × 9 × 1 grid was used for the 3 × 4 × 5 model. These values are presented in Table 1, and they are in good agreement with other reported theoretical calculations[18] and measurements.[11,12]

Similarly, the adsorption energies for each metal on the NiAl(110) surface were computed for all possible adsorption sites using both k-points grids. All differences in the bond lengths were less than 0.02 Å and in adsorption energies less than 6 meV. Therefore, we only used the smallest grid (7 × 9 × 1) for the present study. To obtain the adsorption energies, calculations for the isolated metal atoms were previously carried out, and the resulting electronic ground states were approximately ^{3}D (d^9s^1) for Pt and Pd, and ^{2}S ($d^{10}s^1$) for Cu, Ag, and Au.

For the calculated work function values, a dipole correction[69,70] was added in the surface normal direction. The calculated electrostatic potential for each supercell showed a clear distinction between the vacuum level of each side of the slab. The work function (Φ) values were then calculated using the following equation:

$$\Phi = E_{vac} - E_F \quad (1)$$

where E_{vac} is the electrostatic potential in the vacuum region of the supercell on the adsorbate side and E_F is the energy Fermi level.

RESULTS

Adsorption Sites. The NiAl(110) surface has seven potential adsorption sites as illustrated in Figure 1. There are

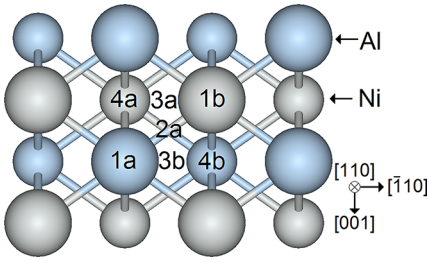

Figure 1. Top view of a (2 × 2) supercell of NiAl(110).

two 4-fold coordinated sites (4a and 4b) with two Ni and two Al atoms; two 3-fold coordinated sites with two Al and one Ni (3a) or two Ni and one Al (3b); one 2-fold coordinated site with one Al and one Ni (2a); and finally, two sites on top of one Al (1a) and one Ni (1b).

Every metal atom was initially placed at each site, and a full geometry optimization process was performed to find the relaxed structure and the adsorption energies. The resulting values are summarized in Figure 2. It is significant the different

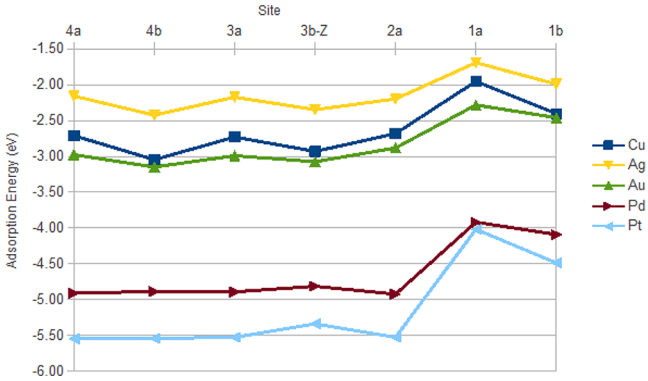

Figure 2. Adsorption energy of different metals (Cu, Ag, Au, Pd, and Pt) on NiAl(110) for the seven potential adsorption sites.

magnitude of the adsorption energy values for atoms from groups 10 and 11. The lower values for group 10 are related to the partial occupation of the d orbitals in opposition to group 11, which has the d states completely filled.

For most cases, the 4b site is the most favorable where the adatom bridges two Ni atoms at shorter distances than the two Al atoms. This is in agreement with other computational studies that also predict that metal adatoms prefer to adsorb on this site named 4b in the present study and also with some experimental evidences.[18,34,35,38−40] The second favorable site for most metals is the 4a, in which the difference with the previous one is that the bridge distances are inverted because the Al−Al distance is shorter than the Ni−Ni distance. The only exceptions are for Pd and Pt with both sites having the same energy.

The three-coordinated site 3a is similar to 4a but with the adatom slightly displaced toward one of the Ni and still bonding to two Al atoms. Site 3b showed to be an unstable site for all metals, and all geometry optimizations ended up with the adatom in a site 4b. For that reason, Figure 2 only reports values regarding the optimized structure constrained along the z axis ([110] direction) and named 3b-Z. Site 2a is stable for group 11 metals, but not for Pd and Pt. For these two cases the relaxation process ended with the adatom in site 3a, and the corresponding two values reported in Figure 2 are for the adsorption structures optimized only along the z axis. Finally, the highest energy sites are one-coordinated on top of one Al (site 1a) or one Ni (site 1b) atom. This relative stability order agrees well with estimates from other studies on Pt,[18] Ag, and Au.[46,50]

All the adsorption energies were computed for one adatom in a (2 × 2) supercell, i.e., a coverage (Θ) of 0.25 monolayer (ML). Additionally, we have analyzed the effect of reducing the coverage on the adsorption structure by using a (3 × 4) surface cell (i.e., Θ = 0.08 ML) to compute the structural parameters

dx.doi.org/10.1021/jp405877k | J. Phys. Chem. A 2014, 118, 5748−5755

Table 2. Atom Properties and Some Structural Parameters for Metal Adatoms on the NiAl(110) Surface; Δ_{11} Represents the Surface Rippling; d(metal) Are the Bond Lengths between the Adatom and the metal; and Δh Are Relative Height Distances

atom	empirical cov. radii (Å)	Pauling elect.	polariz. (a.u.)	surface cell	site	Δ_{11} (Å)	d(Al) (Å)	d(Ni) (Å)	Δh (Å)
Cu	1.38	1.90	45.0	2 × 2	4b	0.19	2.61	2.35	0.07
					4a	−0.05	2.36	2.67	0.15
				3 × 4	4b	0.17	2.60	2.37	0.03
					4a	−0.04	2.37	2.63	0.09
Ag	1.53	1.93	52.2	2 × 2	4b	0.17	2.85	2.59	0.43
					4a	0.08	2.56	2.91	0.44
				3 × 4	4b	0.18	2.81	2.59	0.35
					4a	0.00	2.54	2.87	0.38
Au	1.44	2.54	35.1	2 × 2	4b	0.24	2.72	2.54	0.27
					4a	0.06	2.48	2.89	0.37
				3 × 4	4b	0.21	2.69	2.54	0.19
					4a	0.01	2.47	2.81	0.27
Pd	1.31	2.20	32.0	2 × 2	4b	0.31	2.58	2.49	0.18
					4a	0.06	2.37	2.80	0.25
				3 × 4	4b	0.22	2.56	2.50	0.10
					4a	0.04	2.36	2.74	0.17
Pt	1.28	2.28	44.0	2 × 2	4b	0.29	2.52	2.45	0.06
					4a	0.02	2.34	2.73	0.18
				3 × 4	4b	0.20	2.52	2.46	0.00
					4a	0.01	2.35	2.70	0.12

for sites 4a and 4b, and they are reported in Table 2. It becomes apparent that there are not appreciable differences for both coverages, and the possible lateral interactions between the adsorbed metals at the highest coverage do not alter any structural parameter from the lower coverage.

At both coverages, the metal adsorption induces structural relaxation to some extent. In particular, the surface rippling (Δ_{11}) created in the clean surface (0.17 Å) as a stabilizing effect is altered upon adsorption. In site 4b, all metals tend to increase this distance; Au, Pd, and Pt being the adsorbates that modify the most. Also, for Cu, Ag, and Au, the distances to Al atoms are longer than to Ni atoms by around 0.2 Å, while for Pd and Pt both distances are quite similar.

On the contrary, in site 4a, this rippling is reduced considerably for all cases, and the surface atoms bonded to the monomer ended up approximately at the same height. It can be seen that now distances from the adatom (Ad) to Ni atoms are longer (by around 0.3 Å) than to Al atoms. However, the rippling reduction has the effect of shortening the bond distances to the Ni atoms, and consequently, the length differences between Ad−Ni and Ad−Al are smaller than those expected from a nonrelaxed site. Particularly, for Pd and Pt the bond lengths in both sites 4a and 4b are more similar than for the other metals, justifying the similar adsorption energies.

The heights at which the atoms sit on each site correlate quite well with the empirical covalent atomic radii.[71] Thus, the biggest atom is Ag (1.53 Å) and places at the highest height from the surface forming the longest bonds with Ni and Al atoms. The second one is Au (1.44 Å) followed by Cu (1.38 Å), which shows similar values to Pd (1.31 Å) and finally Pt (1.28 Å).

Projected Density of States. The projected local density of states (LDOS) for the adatom and its nearest neighbors are plotted in Figure 3. The densities of states for all adatoms and Ni are dominated by d bands, and the s and p bands contribute to these plots with very low intensity. For Ag and Au, d states are fully occupied, the bands are narrow, and they arise at lower energy values than Ni d bands. Consequently, the coupling with

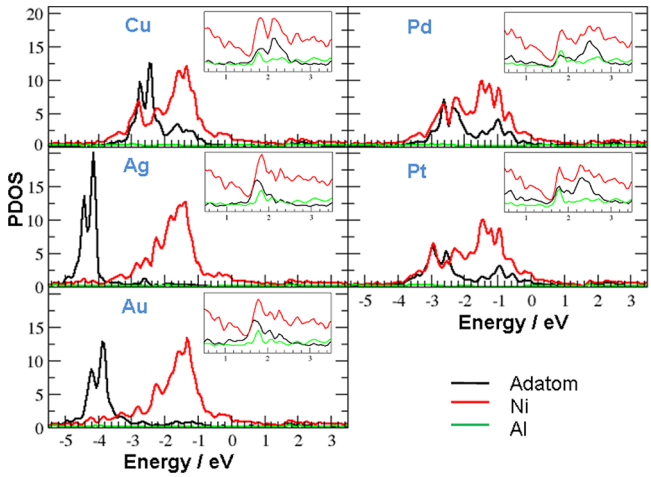

Figure 3. Projected local density of states (LDOS) for each adsorption system at site 4b. The Fermi level is set at 0 eV.

the surface has no appreciable d character but essentially sp character.

Differently, Cu, Pd , and Pt d bands appearing at higher energy values extend over wider energy ranges and hybridize significantly with the Ni d orbitals showing strong covalent contribution. Furthermore, Pd and Pt d bands show significant density of unoccupied states above the Fermi level.

The first feature caused by the adatom above the Fermi level is a resonance state with sp character appearing at 1.75 eV for Ag and Au in good agreement with scanning tunneling spectroscopy measurements,[35] and at slightly higher values for the other metals. This resonance is originated by the hybridization of sp orbitals from the adatom and the Al nearest neighbors. The next feature is a band above 2 eV, which is more intense than the first feature for Cu, Pd, and Pt, and almost negligible for Ag and Au. This resonance is caused from hybridization of adatom sp orbitals with surface Ni states.

Charge Density. To further examine how the metal adsorption affects the electron density of the system, the

dx.doi.org/10.1021/jp405877k | J. Phys. Chem. A 2014, 118, 5748−5755

planar averaged charge density difference plots were calculated in slices perpendicular to the surface normal, following the equation

$$\Delta\rho_z = \rho_z M/\mathrm{NiAl}(110) - \rho_z \mathrm{NiAl}(110) - \rho_z M \quad (2)$$

where $\rho_z M/\mathrm{NiAl}(110)$, $\rho_z \mathrm{NiAl}(110)$, and $\rho_z M$ are the planar averaged density along the z-direction (perpendicular to surface plane) of the adsorption system, the clean surface, and the isolated metal atoms, respectively, all at their positions in the adsorption system.

It can be seen for all cases that the charge density is not evenly distributed throughout the system (see Figure 4). In particular, there is a large accumulation of charge between the adsorbed metal and the topmost Al surface layer, and there are two depletion regions, one around the topmost surface atoms and another above the adatom center of mass. This charge distribution can be understood when considering that all adsorbed atoms are more electronegative than the surface components: Ni (1.91) and Al (1.61). Consequently, it is expected that some charge transfer should occur from the surface to the metal atom to some extent, and this can be seen in a significant depletion region around the surface atoms. Thus, the negatively charged species induce surface polarization in which the surface electron density left is accumulated far away from the adsorbate creating a positive image charge, which is reflected in small positive regions around 3.5 Å corresponding to atoms from the second surface plane. This positive image charge also induces a polarization effect on the adsorbate, attracting its electron density. This is seen in the largest accumulation region between the adatom and the surface, and the depletion region extending from the metal adsorbate into the vacuum. This depletion region correlates precisely with the electron polarizability of the neutral adatom, which for group 11 follows this sequence: Ag (52) > Cu (45) > Au (35), where the polarizability values are expressed in a.u.[72]

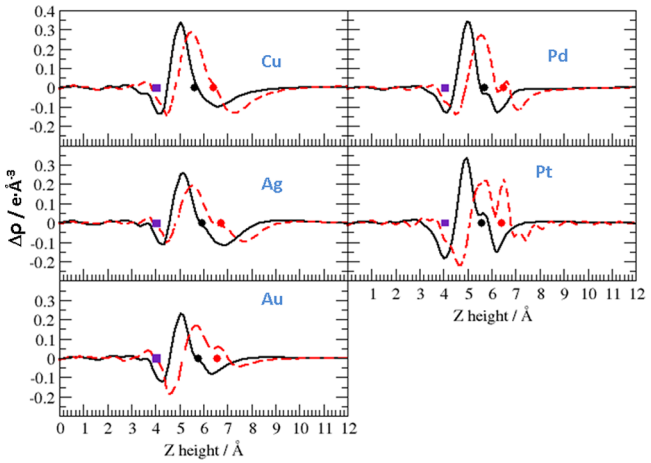

Figure 4. Planar averaged charge density difference plots for metal monomers (Cu, Ag, Au, Pd, and Pt) on NiAl(110) in site 4b at the equilibrium position (black line) and shifted 0.8 Å upward (dashed red line). The square indicates the top layer position, while the black and red dots depict the position of the adatom at equilibrium and shifted.

Electron density difference plots (Figure 5) show the character of these bonds. There is electron density accumulation between each adatom and the two Al surface atoms and depletion regions close to the Al atoms. For group 11, that accumulation is larger for Au, followed by Ag and finally Cu. This agrees well with the electronegativity order of the three metal elements (see Table 2), indicating that the Ad−Al bond is predominantly polar. The same behavior is observed for Pt and Pd, in which the largest accumulation is seen for Pt, which is more electronegative than Pd. However, it becomes clear that the bonds between the metal atom and the Ni surface atoms are more directional. They are formed from d-orbital interactions, and they are mainly covalent. The density charge in these bonds accumulates closer to the adatom, and the Ni d-orbitals appear as depletion density charge regions. This is consistent with the fact that Ni is less electronegative than all the considered metal atoms.

Work Function. Table 3 summarizes the work function changes in sites 4a and 4b for each metal at two coverages. As expected there are not appreciable differences for both sites since they are quite similar 4-fold coordinated sites. The effect of increasing the coverage also leads to a larger work function decrease, being more significant for Ag. This result indicates

Table 3. Work Function Changes (eV) for Each Metal in Sites 4a and 4b Using Surface Models (3 × 4) and (2 × 2), Which Represent Coverages of 0.08 and 0.25 ML, Respectively

surface cell	site	Ag	Au	Cu	Pd	Pt
3 × 4	4a	−0.44	−0.26	−0.33	−0.32	−0.23
	4b	−0.46	−0.28	−0.33	−0.29	−0.21
2 × 2	4a	−0.97	−0.57	−0.70	−0.64	−0.40
	4b	−0.99	−0.60	−0.69	−0.57	−0.38

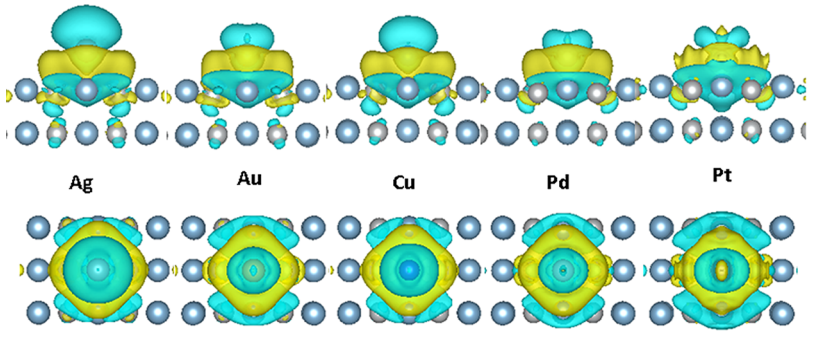

Figure 5. Charge density difference plots (generated using VESTA software[73]) for metal monomers (Cu, Ag, Au, Pd, and Pt) on NiAl(110) in site 4b. Top figures are side views, while bottom images show the top views. Surface Al and Ni atoms in blue and gray spheres, respectively. Yellow regions show charge accumulation, and blue regions represent charge loss. The iso-surface value is 0.002 Bohr^{-3}.

dx.doi.org/10.1021/jp405877k | J. Phys. Chem. A 2014, 118, 5748−5755

that at 0.25 ML the lateral adatom interactions, although do not induce energetic or structural changes as seen above, modify the electronic structure importantly. For that reason, the electronic properties discussed below will refer to the lowest coverage (0.08 ML).

All values that correspond to work function decreases, which following the general rule, would be related to charge transfer processes from the adsorbate to the surface. This behavior is opposite to that expected from the electronegativity differences between the metals and the surface, which particularly for Au and Pt would indicate a charge transfer from the surface to the adsorbate.

Additionally, the change in the surface dipole moment, $\Delta\mu$ (in Debye), induced by the adsorbate has been calculated by the Helmholtz equation

$$\Delta\mu = \frac{\Delta\Phi A}{12\pi\Theta} \tag{3}$$

where A is the area in Å^2 per (1×1) surface unit cell, $\Delta\Phi$ is the work-function change in eV, and Θ is the surface coverage.[74] Obviously, the results (Table 4) also indicate the formation of significant negative surface dipole moments.

Table 4. Comparison of Different Estimates of the Effect of the Adsorption of the Adatom on NiAl(110), for Two Adatom Positions: at Equilibrium, and an Upward Shift of 0.8 Å. Values of Surface Dipole (D), Work Function Change (eV), Bader Charge (e), and Surface Charge (e). (Details in the Text)

	z-shift (Å)	Ag	Au	Cu	Pd	Pt
surface dipole (D)	0.0	−1.75	−1.07	−1.26	−1.10	−0.80
	0.8	−2.13	−0.61	−1.64	−1.10	−0.42
work function change (eV)	0.0	−0.46	−0.28	−0.33	−0.29	−0.21
	0.8	−0.56	−0.16	−0.43	−0.29	−0.11
Bader charge (e)	0.0	0.11	0.44	0.41	−0.23	0.41
	0.8	−0.10	0.30	−0.01	−0.14	0.23
surface charge (e)	0.0	−0.56	−0.62	−0.76	−0.81	−1.17
	0.8	−0.50	−1.04	−0.65	−1.03	−1.16

To gain insight into the origin of this anomaly, we have analyzed the electronic structure when moving the adsorbate from the equilibrium position along the z-coordinate by 0.2 Å up to 0.8 Å. Figure 4 illustrates the planar averaged density plots for both at the equilibrium height (solid black line) and at the metal atom height moved upward by 0.8 Å (dashed red line). At this displaced position, the charge variation effects become clearer. Thus, for this situation, there is a first depletion area associated to the charge transferred from the surface atoms to the interface region characterized by a broad area of charge accumulation (first positive peak). Also, it can be seen that at the displaced adsorbate position, a second peak of accumulation charge becomes more prominent for Au and Pt, which are the most electronegative atoms. This charge corresponds partially to the weak polarization of their own charge (associated to the second depletion charge area) and more importantly to the charge transferred from the surface. On the contrary, the less electronegative atoms (Ag, Cu, and Pd) still exhibit a significant depletion charge area from the polarization effect, and this charge is accumulated in the intermediate region between the surface atoms and the adsorbate instead of localized on the latter one.

The work function changes at the higher height diminish for Ag and Cu (the most polarizable atoms) in agreement with the negative induced moment changes, while for Au and Pt the variations go in the opposite direction. For Pd, although the induced moment decreases, the value of work function change is the same as that for the equilibrium height.

Therefore, the metal shift upward provokes in the most polarizable and less electronegative adatoms (Ag and Cu) a reduction in the charge transfer from the surface and a polarization increase leading to a larger negative induced moment and work function change. However, that shift induces in the less polarizable atoms (Au and Pt) a lowering in the polarization effect, and because of the high electronegativity, the charge transfer is still effective resulting in the general electronegative adsorbate behavior with reduced negative induced surfaces moment and work function change. Finally, Pd has an intermediate behavior and despite its high electronegativity is still polarizable enough to show similar values of negative induced moment and work function change than at the equilibrium height.

A reasonable estimate of the charge transfer from the surface to the adsorbate can be computed from integrating the first large depletion area around the surface atoms (see Figure 4). Table 4 shows that the largest charge transfers are for Pd and Pt, and that would mainly correspond to the d-bonds. For the group 11 metals, Cu obtains more charge from the surface due to a better hybridization with the Ni d-orbitals, whereas Ag and Au interact with the surface essentially through the sp-orbitals with the Al atoms.

Another way to estimate the charge transfer is using the Bader analysis, which is based on finding the critical points of charge density in order to divide the 3D space into volumes assigned to the different atoms. The charge associated to each atom is computed from the integration of the charge density in the corresponding volume.[75] Although some caution must be taken when considering the absolute values of Bader charges, they become useful for finding general trends when comparing different systems in analogous situations.

The computed Bader charges predict maxima values and similar accumulation charges for Cu, Au, Pt, still some accumulation for Ag, and loss charge for Pd. These values reflect accordingly that all adsorbates take charge from the surface except Pd. It is interesting to compare with the corresponding values when the adatom moves upward. On doing so, the effects of the electronegativity and polarization are diminished and only the most significant one dominates. Thus, Bader charges for the most polarizable metals (Ag and Cu) are negative indicating that at this height these atoms lose electron density, while for the most electronegative atoms (Au and Pt) they still predict a smaller gain charge around the adatom than for the equilibrium position. Whereas for Pd the charge value is still negative indicating that at both distances the charge density arising from the surface and the metal is distributed equally in the intermediate region (see Figure 3) leading to more covalent bonds.

CONCLUSIONS

In this work we have carried out a density functional study of different transition metal (Pd, Pt, Cu, Ag, and Au) atoms adsorbed on the NiAl(110) surface. The adsorption sites have been characterized considering two different surface models: (2

dx.doi.org/10.1021/jp405877k | J. Phys. Chem. A 2014, 118, 5748−5755

× 2) and (3 × 4) cells, which correspond to surface coverages of 0.25 and 0.08 ML, respectively. Both energetically and structurally, negligible differences were found for both systems. All adatoms prefer to sit on a 4-fold coordinated site (4b) binding two Ni and two Al surface atoms. The metal adsorption in this site induces a structural surface relaxation increasing the surface rippling. The nature of the bonding has been studied from the LDOS and charge density differences. Each adatom interacts with the Al atoms through sp orbitals forming polar bonds in which the charge accumulation is controlled by the electronegativity differences being more significant for the most electronegative atoms (Au and Pt). The interaction with the Ni atoms is predominantly via d-orbitals, giving rise to more directional covalent bonds. LDOS plots show that the adatoms and Ni d bands overlap widely for Cu, Pt, and Pd, but not for Au and Ag. According to the higher electronegativies of the adatoms compared to the Ni and Al atoms, charge transfer processes from the surface to the adsorbate would be expected and the related work function changes would be positive. All calculated values are negative due to the polarization of the negatively charged adsorbates by the positive surface image, created after adsorption and leading to a negative induced surface moment. For the atoms (Ag and Cu) with similar electronegativity than Ni, this polarization effect is more notorious leading to larger work function changes but less important charge transfer processes. A model where the adatoms are put further from the surface has allowed to observe different behaviors in terms of change transfer and surface dipole formation for the most polarizable metals (Ag and Cu), for the most electronegative ones (Au and Pt), and for Pd atom with an intermediate behavior.

AUTHOR INFORMATION

Corresponding Author

*(E.D.S.) E-mail: zacarias@ifi.unicamp.br. Phone: +55 (19) 3521 5491. Fax: +55 (19) 3521 3137.

Notes

The authors declare no competing financial interest.

ACKNOWLEDGMENTS

M.A.S. would like to thank CAPES for providing a grant to support a stay at Institute of Physics "Gleb Wataghin", UNICAMP. E.P.M.A would like to thank FAPESP for providing the post-doctoral grant. This research had the financial support of FAPESP, CNPq, CAPES, and FAEPEX-UNICAMP. The calculations were performed at the National Center for High Performance Computing in Sao Paulo (CENAPAD-SP).

REFERENCES

(1) Sinfelt, J. H. *Bimetallic Catalysts: Discoveries, Concepts, Applications*; Wiley: New York, 1983.

(2) Stierle, A.; Renner, F.; Streitel, R.; Dosch, H.; Drube, W.; Cowie, B. C. X-ray Diffraction Study of the Ultrathin Al_2O_3 Layer on NiAl(110). *Science* **2004**, *303*, 1652−1656.

(3) Kresse, G.; Schmid, M.; Napetschnig, E.; Shishkin, M.; Kohler, L.; Varga, P. Structure of the Ultrathin Aluminum Oxide Film on NiAl(110). *Science* **2005**, *308*, 1440−1442.

(4) Lozovoi, A. Y.; Alavi, A.; Finnis, M. W. Surface Stoichiometry and the Initial Oxidation of NiAl(110). *Phys. Rev. Lett.* **2000**, *85*, 610−613.

(5) Lozovoi, A. Y.; Alavi, A.; Finnis, M. W. Surface Energy and the Early Stages of Oxidation of NiAl(110). *Comput. Phys. Commun.* **2001**, *137*, 174−194.

(6) Finnis, M. W.; Lozovoi, A. Y.; Alavi, A. The Oxidation of NiAl: What Can We Learn from Ab Initio Calculations? *Annu. Rev. Mater. Res.* **2005**, *35*, 167−207.

(7) Leyens, C.; Pint, B. A.; Wright, I. G. Effect of Composition on the Oxidation and Hot Corrosion Resistance of NiAl Doped with Precious Metals. *Surf. Coat. Technol.* **2000**, *133*−*134*, 15−22.

(8) Carling, K. M.; Carter, E. A. Effects of Segregating Elements on the Adhesive Strength and Structure of the α-Al_2O_3/β-NiAl Interface. *Acta Mater.* **2007**, *55*, 2791−2803.

(9) Huntz, A. M. Influence of Active Elements on the Oxidation Mechanism of M-CR-AL Alloys. *Mater. Sci. Eng.* **1987**, *87*, 251−260.

(10) Prescott, R.; Graham, M. J. The Formation of Aluminum-Oxide Scales on High-temperature Alloys. *Oxid. Met.* **1992**, *38*, 233−254.

(11) Davis, H. L.; Noonan, J. R. Rippled Relaxation in the (110) Surface of the Ordered Metallic Alloy NiAl. *Phys. Rev. Lett.* **1985**, *54* (6), 566−569.

(12) Yalisove, S. M.; Graham, W. R. Multilayer Rippled Structure of the NiAl(110) Surface: a Medium Energy Ion Scattering Study. *Surf. Sci.* **1987**, *183*, 556−564.

(13) Kang, M. H.; Mele, E. J. NiA1(110) Surface: First-Principles Determination of the Rippled Relaxation. *Phys. Rev. B* **1987**, *36*, 7371−7377.

(14) Lee, J. I.; Fu, C. L.; Freeman, A. J. All-Electron Local-Density Theory of the Rippled NiAl(110) Surface. *Phys. Rev. B* **1987**, *36*, 9318−9321.

(15) Lui, S.-C.; Kang, M. H.; Mele, E. J.; Plummer, E. W.; Zehner, D. M. Surface States on NiA1(110). *Phys. Rev. B* **1989**, *39*, 13149−13159.

(16) Hansen, K. H.; Gottschalck, J.; Petersen, L.; Hammer, B.; Laegsgaard, E.; Besenbacher, F.; Stensgaard, I. Surface Waves on NiAl(110). *Phys. Rev. B* **2001**, *63*, 115421.

(17) Song, Z.; Pascual, J. I.; Conrad, H.; Horn, K.; Rust, H.-P. Imaging Surface Electronic Structure of NiAl(110) using Low-Temperature Scanning Tunneling Microscopy. *Appl. Phys. A: Mater. Sci. Process.* **2001**, *72*, S159−S162.

(18) Carling, K. M.; Glover, W.; Gunaydin, H.; Mitchell, T. A.; Carter, E. A. Comparison of S, Pt, and Hf Adsorption on NiAl(110). *Surf. Sci.* **2006**, *600*, 2079−2090.

(19) Kogita, T.; Kohyama, M.; Kido, Y. Structure and Dynamics of NiAl(110) Studied by High-Resolution Ion Scattering Combined with Density Functional Calculations. *Phys. Rev. B* **2009**, *80*, 235414.

(20) Lerch, D.; Dossel, K.; Hammer, L.; Muller, S. Point Defects in the NiAl(100) Surface. *J. Phys.: Condens. Matter* **2009**, *21*, 134007.

(21) Saadi, S.; Hinnemann, B.; Appel, C. C.; Helveg, S.; Abild-Pedersen, F.; Nørskov, J. K. First-Principles Investigations of Ni_3Al(111) and NiAl(110) Surfaces at Metal Dusting Conditions. *Surf. Sci.* **2011**, *605*, 582−592.

(22) Hanbicki, A. T.; Baddorf, A. P.; Plummer, E. W.; Hammer, B.; Scheffler, M. The Interaction of Hydrogen with the (110) Surface of NiAl. *Surf. Sci.* **1995**, *331*, 811−817.

(23) Sein, L. T., Jr.; Jansen, S. A. DFT Study of the Adsorption and Dissociation of Methanol on NiAl(100). *J. Catal.* **2000**, *196*, 207−211.

(24) Sheu, B.; Chaturvedi, S.; Strongin, D. R. Adsorption and Decomposition of Methanol on NiAl(110). *J. Phys. Chem.* **1994**, *98*, 10258−10268.

(25) Svenum, I.-H.; Borck, Ø.; Schulte, K.; Walle, L. E.; Borg, A. Adsorption of Methanol on Ni_3Al(111) and NiAl(110): A High Resolution PES Study. *Surf. Sci.* **2009**, *603*, 2370−2377.

(26) Borck, Ø.; Svenum, I.-H.; Borg, A. Adsorption of Methanol and Methoxy on NiAl(110) and Ni_3Al(111): A DFT Study. *Surf. Sci.* **2009**, *603*, 2378−2386.

(27) Freund, H. -J.; Kuhlenbeck, H.; Staemmler, V. Oxide Surfaces. *Rep. Prog. Phys.* **1996**, *59*, 283−347.

(28) Hansen, K. H.; Worren, T.; Stempel, S.; Lægsgaard, E.; Bäumer, M.; Freund, H.-J.; Besenbacher, F.; Stensgaard, I. Palladium Nanocrystals on Al_2O_3: Structure and Adhesion Energy. *Phys. Rev. Lett.* **1999**, *83*, 4120−4123.

(29) Kulawik, M.; Nilius, N.; Freund, H.-J. Influence of the Metal Substrate on the Adsorption Properties of Thin Oxide Layers: Au

Atoms on a Thin Alumina Film on NiAl(110). *Phys. Rev. Lett.* **2006**, *96*, 036103.
(30) Nilius, N.; Ganduglia-Pirovano, M. V.; Brázdová, V.; Kulawik, M.; Sauer, J.; Freund, H. J. Electronic Properties and Charge State of Gold Monomers and Chains Adsorbed on Alumina Thin Films on NiAl(110). *Phys. Rev. B* **2010**, *81*, 045422.
(31) Napetschnig, E.; Schmid, M.; Varga, P. Pd, Co and Co−Pd Clusters on the Ordered Alumina Film on NiAl(110): Contact Angle, Surface Structure and Composition. *Surf. Sci.* **2007**, *601*, 3233−3245.
(32) Nilius, N.; Wallis, T. M.; Ho, W. Development of One-Dimensional Band Structure in Artificial Gold Chains. *Science* **2002**, *297*, 1853−1856.
(33) Nilius, N.; Wallis, T. M.; Ho, W. Vibrational Spectroscopy and Imaging of Single Molecules: Bonding of CO to Single Palladium Atoms on NiAl(110). *J. Chem. Phys.* **2002**, *117*, 10947−10952.
(34) Nilius, N.; Wallis, T. M.; Persson, M.; Ho, W. Distance Dependence of the Interaction between Single Atoms: Gold Dimers on NiAl(110). *Phys. Rev. Lett.* **2003**, *90*, 196103.
(35) Wallis, T. M.; Nilius, N.; Ho, W. Single Molecule Vibrational and Electronic Analyses of the Formation of Inorganic Complexes: CO Bonding to Au and Ag Atoms on NiAl(110). *J. Chem. Phys.* **2003**, *119*, 2296−2300.
(36) Nilius, N.; Wallis, T. M.; Ho, W. Realization of a Particle-in-a-Box: Electron in an Atomic Pd Chain. *J. Phys. Chem. B* **2005**, *109*, 20657−20660.
(37) Wallis, T. M.; Nilius, N.; Ho, W. Electronic Density Oscillations in Gold Atomic Chains Assembled Atom by Atom. *Phys. Rev. Lett.* **2002**, *89*, 236802.
(38) Persson, M. Computational Study of Electron States in Au Chains on NiAl(110). *Phys. Rev. B* **2004**, *70*, 205420.
(39) Calzolari, A.; Nardelli, M. B. First Principles Theory of Artificial Metal Chains on NiAl(110) Surface. *Phys. Rev. B* **2005**, *72*, 045416.
(40) Lee, H. J.; Ho, W.; Persson, M. Spin Splitting of s and p States in Single Atoms and Magnetic Coupling in Dimers on a Surface. *Phys. Rev. Lett.* **2004**, *92*, 186802.
(41) Evecen, M.; Çakmak, M. Adsorption of S, O, and H on the NiAl(110)-(2 × 2) Surface. *Phys. B* **2010**, *405*, 4059−4063.
(42) Persson, M. Adsorption-Induced Constraint on Delocalization of Electron States in an Au Chain on NiAl(110). *Phys. Rev. B* **2005**, *72*, 081404.
(43) Calzolari, A.; Cavazzoni, C.; Nardelli, M. B. Electronic and Transport Properties of Artificial Gold Chains. *Phys. Rev. Lett.* **2004**, *93*, 096404.
(44) Oncel, N. Atomic Chains on Surfaces. *J. Phys.: Condens. Matter* **2008**, *20*, 393001.
(45) Unal, B.; Qin, F.; Han, Y.; Liu, D.-J.; Jing, D.; Layson, A. R.; Jenks, C. J.; Evans, J. W.; Thiel, P. A. Scanning Tunneling Microscopy and Density Functional Theory Study of Initial Bilayer Growth of Ag Films on NiAl(110). *Phys. Rev. B* **2007**, *76*, 195410.
(46) Han, Y.; Ünal, B.; Qin, F.; Jing, D.; Jenks, C. J.; Liu, D.-J.; Thiel, P. A.; Evans, J. W. Kinetics of Facile Bilayer Island Formation at Low Temperature: Ag/NiAl(110). *Phys. Rev. Lett.* **2008**, *100*, 116105.
(47) Han, Y.; Ünal, B.; Jing, D.; Qin, F.; Jenks, C. J.; Liu, D.-J.; Thiel, P. A.; Evans, J. W. Formation and Coarsening of Ag(110) Bilayer Islands on NiAl(110): STM Analysis and Atomistic Lattice-Gas Modeling. *Phys. Rev. B* **2010**, *81*, 115462.
(48) Han, Y.; Jing, D.; Ünal, B.; Qin, F.; Thiel, P. A.; Evans, J. W. Far-from-equilibrium Film Growth on Alloy Surfaces: Ni and Al on NiAl(110). *Phys. Rev. B* **2011**, *84*, 113414.
(49) Han, Y.; Ünal, B.; Evans, J. W. Formation of a Novel Ordered Ni_3Al Surface Structure by Codeposition on NiAl(110). *Phys. Rev. Lett.* **2012**, *108*, 216102.
(50) Duguet, T.; Han, Y.; Yuen, C.; Jing, D.; Unal, B.; Evans, J. W.; Thiel, P. A. Self-Assembly of Metal Nanostructures on Binary Alloy Surfaces. *Proc. Natl. Acad. Sci.* **2011**, *108*, 989−994.
(51) Delcher, T. A.; Ehrlich, G. Chemisorption on Single-Crystal Planes: Nitrogen on Tungsten. *J. Chem. Phys.* **1965**, *42*, 2686−2702.
(52) Adams, D. L.; Germer, L. H. Adsorption on Single-Crystal Planes of Tungsten: I. Nitrogen. *Surf. Sci.* **1971**, *27*, 21−44.
(53) Holscher, A. A. Surface Potentials of Nitrogen on Individual Crystal Faces of Tungsten. *J. Chem. Phys.* **1964**, *41*, 579.
(54) Michaelides, A.; Hu, P.; Lee, M.-H.; Alavi, A.; King, D. A. Resolution of an Ancient Surface Science Anomaly: Work Function Change Induced by N Adsorption on W100. *Phys. Rev. Lett.* **2003**, *90*, 246103.
(55) Pettersson, L. G. M.; Bagus, P. S. Adsorbate Ionicity and Surface-Dipole-Moment Changes: Cluster-Model Studies of Cl/Cu(100) and F/Cu(100). *Phys. Rev. Lett.* **1986**, *56*, 500−503.
(56) Yang, Y.; Yarmoff, J. A. Effects of Adsorbates on Charge Exchange in Li^+ Ion Scattering from Ni(100). *J. Vac. Sci. Technol., A* **2003**, *21* (4), 1317−1321.
(57) Jo, S. K.; White, J. M. Characterization of Adsorption States of Atomic Iodine on Pt(111). *Surf. Sci.* **1992**, *261*, 111−117.
(58) Migani, A.; Sousa, C.; Illas, F. Chemisorption of Atomic Chlorine on Metal Surfaces and the Interpretation of the Induced Work Function Changes. *Surf. Sci.* **2005**, *574*, 297−305.
(59) Leung, T. C.; Kao, C. L.; Su, W. S.; Feng, Y. J.; Chan, C. T. Relationship Between Surface Dipole, Work Function and Charge Transfer: Some Exceptions to an Established Rule. *Phys. Rev. B* **2003**, *68*, 195408.
(60) Kresse, G.; Hafner, J. Ab initio Molecular Dynamics for Liquid Metals. *Phys. Rev. B* **1993**, *47*, 558−561.
(61) Kresse, G.; Furthmuller, J. Efficiency of Ab-Initio Total Energy Calculations for Metals and Semiconductors using a Plane-Wave Basis Set. *Comput. Mater. Sci.* **1996**, *6*, 15−50.
(62) Kresse, G.; Furthmuller, J. Efficient Iterative Schemes for ab Initio Total-Energy Calculations Using a Plane-Wave Basis Set. *Phys. Rev. B* **1996**, *54*, 11169−11186.
(63) Payne, M. C.; Teter, M. P.; Allan, D. C.; Arias, T. A.; Joannopoulos, J. D. Iterative Minimization Techniques for ab Initio Total-Energy Calculations: Molecular-Dynamics and Conjugate Gradients. *Rev. Mod. Phys.* **1992**, *64*, 1045−1097.
(64) Blochl, P. E. Projector Augmented-Wave Method. *Phys. Rev. B* **1994**, *50*, 17953−17979.
(65) Kresse, G.; Joubert, D. From Ultrasoft Pseudopotentials to the Projector Augmented-Wave Method. *Phys. Rev. B* **1999**, *59*, 1758−1775.
(66) Perdew, J. P. In *Electronic Structure of Solids '91*; Ziesche, P., Eschrig, H., Eds.; Akademie Verlag: Berlin, Germany, 1991.
(67) Perdew, J. P.; Chevary, J. A.; Vosko, S. H.; Jackson, K. A.; Pederson, M. R.; Singh, D. J.; Fiolhais, C. Atoms, Molecules, Solids, and Surfaces: Applications of the Generalized Gradient Approximation for Exchange and Correlation. *Phys. Rev. B* **1992**, *46*, 6671−6687.
(68) Kittel, C. *Introduction to Solid State Physics*; John Wiley and Sons: New York, 1986.
(69) Makov, G.; Payne, M. C. Periodic Boundary-Conditions in ab-Initio Calculations. *Phys. Rev. B* **1995**, *51*, 4014−4022.
(70) Neugebauer, J.; Scheffler, M. Adsorbate−Substrate and Adsorbate−Adsorbate Interactions of Na and K Adlayers on Al(111). *Phys. Rev. B* **1992**, *46*, 16067−16080.
(71) Periodic Table of the Elements. http://www.webelements.com/.
(72) Schwerdtfeger, P.; Bowmaker, G. A. Relativistic Effects in Gold Chemistry. V. Group 11 Dipole Polarizabilities and Weak Bonding in Monocarbonyl Compounds. *J. Chem. Phys.* **1994**, *100*, 4487−4497.
(73) Momma, K.; Izumi, F. VESTA 3 for Three-Dimensional Visualization of Crystal, Volumetric and Morphology Data. *J. Appl. Crystallogr.* **2011**, *44*, 1272−1276.
(74) Li, W.-X.; Stampfl, C.; Scheffler, M. Oxygen Adsorption on Ag(111): A Density-Functional Theory Investigation. *Phys. Rev. B* **2002**, *65*, 075407−1−19.
(75) Tang, W.; Sanville, E.; Henkelman, G. A Grid-Based Bader Analysis Algorithm without Lattice Bias. *J. Phys.: Condens. Matter* **2009**, *21*, 084204.